Strongly Tilted Field Induced Hamiltonian Dimerization and Nested Quantum Scars in the 1D Spinless Fermi–Hubbard Model

Wei-Jie Huang[1,2,3], Yu-Biao Wu[4*], Guang-Can Guo[1,2,3], Wu-Ming Liu[4], and Xu-Bo Zou[1,2,3*]

[1]*Chinese Academy of Sciences Key Laboratory of Quantum Information, University of Science and Technology of China, Hefei 230026, China*
[2]*Chinese Academy of Sciences Center For Excellence in Quantum Information and Quantum Physics, University of Science and Technology of China, Hefei 230026, China*
[3]*Hefei National Laboratory, University of Science and Technology of China, Hefei 230088, China*
[4]*Beijing National Laboratory for Condensed Matter Physics, Institute of Physics, Chinese Academy of Sciences, Beijing 100190, China*

(Received 8 May 2025; accepted manuscript online 1 July 2025)

We investigate the quantum dynamics of the 1D spinless Fermi–Hubbard model with a linear-tilted potential. Surprisingly in a strong resonance regime, we show that the model can be described by the kinetically constrained effective Hamiltonian, and it can be spontaneously divided into two commuting parts dubbed Hamiltonian dimerization, which are composed of two distinct sets of constrained nearest-neighbor hopping terms: one set acting exclusively on odd bonds and the other on even bonds. Specifically it is shown that each part can be independently mapped onto the well-known PXP model; therefore the dimerized Hamiltonian is equivalent to a two-fold PXP model. As a consequence, we numerically demonstrate this system can host the so-called quantum many-body scars, which present dynamical revivals and ergodicity-breaking behaviors. However, in sharp contrast with traditional quantum many-body scars, here the scarring states in our model driven by different parts of the Hamiltonian will revive in different periods, and those of double parts can display a biperiodic revival pattern, both originating from the Hamiltonian dimerization. Besides, the condition of off-resonance is also discussed, and we show the crossover from quantum many-body scar to ergodicity breaking is diagnosed via level statistics. Our model provides a platform for understanding the interplay of Hilbert space fragmentation and the constrained quantum systems.

DOI: 10.1088/0256-307X/42/8/080604 CSTR: 32039.14.0256-307X.42.8.080604

1. Introduction. The rapid experimental progress of recent years in the preparation and controllability of quantum coherent systems has enabled the realization of quantum many-body systems in well-isolated settings and the investigation of their nonequilibrium dynamics, mainly utilizing cold atoms,[1–4] trapped ions,[5–7] and superconducting circuits.[8–11] The most common many-body systems reach their thermal equilibrium under long unitary time evolution, which can be explained by the eigenstate thermalization hypothesis (ETH).[12–14] It states that the expectation value of local observables only depends on the eigenstates, behaving as a basic thermal ensemble for quantum ergodicity. Most quantum many-body systems are known to obey ETH. However, some systems have been proposed that violate ETH, for instance, exactly solvable systems with fixed parameters or many-body localization phases with strong disorders.[15–21]

More recently, another new mechanism of ETH violation called quantum many-body scar (QMBS)[22–31] has been reported in a Rydberg atom quantum simulator, where the majority of the initial states reach the corresponding thermal ensembles, while some special initial states show long-lived revival.[32] Soon afterward, this system was pointed out theoretically to be described by the so-called PXP model.[33–37] Various theoretical explanations for the underlying mechanism have been proposed to investigate the ubiquity of QMBS.[38–44] Later, QMBS has also been found to exist in other kinds of models, such as the Affleck–Kennedy–Lieb–Tasaki model and the spin-1 XY model.[30,41,45–47]

It has been proposed that ergodicity breaking can occur due to the Hilbert space fragmented into exponentially many disconnected subsectors, which typically results from the presence of constrained hopping terms and higher-moment symmetry, such as dipole conservation.[48–51] Furthermore, Hilbert space fragmentation as well as the induced QMBS have been investigated and observed in the spinful fermionic and hard-core bosonic Hubbard models with an applied gradient field.[52,53] In these models, constrained hopping between two consecutive sites is responsible for the ergodicity breaking. A natural follow-up question arises: could constrained hopping terms beyond nearest neighbors lead to novel phenomena in such systems?

In this paper, we investigate the nonergodic behaviors

*Corresponding authors. Email: wuyb@iphy.ac.cn; xbz@ustc.edu.cn
© 2025 Chinese Physical Society and IOP Publishing Ltd. All rights, including for text and data mining, AI training, and similar technologies, are reserved.

in the 1D strongly tilted spinless Fermi–Hubbard model, which exhibits QMBS with quite a few unique features compared with the aforementioned models. We show that the kinetically constrained effective Hamiltonian can be spontaneously divided into two commuting parts acting on four consecutive sites, which can be divided into the isolated odd and even part of Hamiltonian, dubbed Hamiltonian dimerization. Each isolated Hamiltonian part can be mapped to the PXP model. This mapping is achieved by identifying the allowed four-site configurations in the original model with the three-site configurations characteristic of the PXP model.[33] Therefore each part can independently give rise to QMBS, showing long-lived period revivals and ergodicity-breaking many-body eigenstates. The dimerization splits the system into two independent chains, analogous to decoupled ladders. Each chain hosts QMBS similar to the PXP model, leading to nonergodic dynamics. However, initial states overlapping both chains require synchronization between the two subsystems for revivals, hence the dependence on both parts. In particular, if the two individual periods have a considerable difference in size, additional persistent revivals over one large period will emerge. These unique phenomena can be explained by the two isolated parts of Hamiltonian contributing to the two-fold PXP model and, in turn, verifying the Hamiltonian dimerization. We further show that the scarred states rapidly disappear when the tilted potential presents finite detuning with the interaction strength.

2. Hamiltonian Dimerization. We start from the 1D tilted spinless Fermi–Hubbard model governed by the Hamiltonian

$$H = -\frac{J_{\rm o}}{2}\sum_{j=1} c^{\dagger}_{2j+1}c_{2j+2} - \frac{J_{\rm e}}{2}\sum_{j} c^{\dagger}_{2j}c_{2j+1} + \text{H.c.} + \Delta\sum_{j}^{L} j\left(n_j - \frac{1}{2}\right) + U\sum_{j=1}^{L-1}\left(n_j - \frac{1}{2}\right)\left(n_{j+1} - \frac{1}{2}\right). \quad (1)$$

Here L is the system size, $c^{\dagger}_j$ (c_j) denotes the fermion creation (annihilation) operator at site j with the number operator $n_j = c^{\dagger}_j c_j$, $J_{\rm o}$ ($J_{\rm e}$) is the strength of hopping that acts on the odd (even) bonds, U denotes the nearest-neighbor interaction strength, and H.c. stands for the Hermitian conjugation. The tilted potential Δ can be generated by applying a magnetic field gradient along the optical lattice as shown in Fig. 1(a), which introduces a dipole term. In the following, the calculations are performed in open boundary conditions. We focus on the strong-tilted field and resonance regime $\Delta = U \gg J_{\rm o}, J_{\rm e}$. In the rotating frame $H_{\rm eff} = \mathcal{U}H\mathcal{U}^{\dagger} - i\mathcal{U}\partial_t\mathcal{U}^{\dagger}$ ($\mathcal{U}$ is the unitary operator) and rotating wave approximation [see Supplementary Materials (SM)], the Hamiltonian reduces to $H_{\rm eff} = H_{\rm odd} + H_{\rm even}$ with

$$H_{\rm odd} = -\frac{J_{\rm o}}{2}\sum_{j} n_{2j}c^{\dagger}_{2j+1}c_{2j+2}(1 - n_{2j+3}) + \text{H.c.},$$
$$H_{\rm even} = -\frac{J_{\rm e}}{2}\sum_{j} n_{2j-1}c^{\dagger}_{2j}c_{2j+1}(1 - n_{2j+2}) + \text{H.c.}, \quad (2)$$

where $H_{\rm odd}$ and $H_{\rm even}$ denote the constrained hopping terms acting on odd and even bonds respectively, as shown in Fig. 1(a). The hopping between the two middle sites is only permitted when the left surrounded site is occupied and the right surrounded site is empty. In what follows, we use $|1\rangle$ to refer to the occupied state and $|0\rangle$ to refer to the vaccum state.

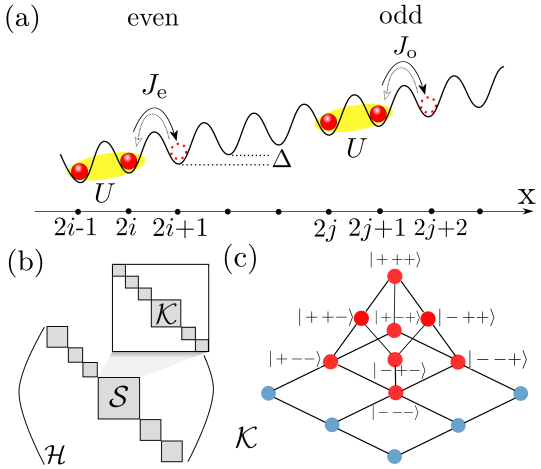

Fig. 1. (a) Schematic of the physical system, Δ is the on-site potential energy, $J_{\rm o}(J_{\rm e})$ is the hopping term acting on odd (even) bonds, and U is the interaction term. Here "..., 2i-1, 2i, 2i+1, ..." stands for the sites on the lattice. (b) The graph represents the illustration of Hilbert-space fragmentation. The symmetry sectors $\mathcal{S}$ of the total Hilbert space $\mathcal{H}$ decouple into disconnected subsectors $\mathcal{K}$. (c) The restricted Hilbert space graph of the effective model (the largest $\mathcal{K}$) for $L = 12$. Red vertices denote the states hopping inside cells and the blue vertices denote the states hopping between cells. We take the value $|+\rangle = |1100\rangle$ ($|-\rangle = |1010\rangle$) and $|1\rangle$ is referred to as the occupied state ($|0\rangle$ is referred to as the vaccum state).

The effective Hamiltonian (2) has two conserved quantities (see SM), which organize the Hilbert space $\mathcal{H}$ into small symmetry sectors $\mathcal{S}$. Because of the hopping process constraint, the Hilbert space in the symmetry sector can be further fractured into many disconnected subsectors $\mathcal{K}$.[54] The corresponding process of Hilbert space fragmentation is shown in Fig. 1(b). Under specific hopping constraints, the Hilbert space fragments into disconnected subsectors. Within each sector, only certain four-site configurations (such as $|1100\rangle$ and $|1010\rangle$) are dynamically accessible, while transitions to other configurations (such as $|1001\rangle$) are forbidden. It is noted that both the two allowed four-site configurations only support the hopping process of the middle two sites, whereas they cannot generate the hopping process of the left or right one site, regardless of the kind of configuration added to the ends. Therefore, the total effective Hamiltonian can be spontaneously divided into two isolated parts, i.e., $H_{\rm odd}$ and $H_{\rm even}$, according to the contained hopping terms acting on odd or even bonds, as shown in Fig. 1(a). Thus, we call it Hamiltonian dimerization.

Dimerized Hamiltonians $H_{\rm odd}$ and $H_{\rm even}$ satisfy the commutation relation $[H_{\rm odd}, H_{\rm even}] = 0$; their combined action leads to distinctive dynamical behaviors. As shown in Table 1, we classify the dynamics into four categories based on the system's hopping patterns.

Table 1. Dynamics based on system's hopping pattern is controlled by $H_{\rm odd}$ or $H_{\rm even}$, according to the Hamiltonian dimerization. We also provide example states for different parts.

$H_{\rm odd}$	$H_{\rm even}$	Example state
✓	×	$\|01100110\cdots\rangle$
×	✓	$\|11001100\cdots\rangle$
✓	✓	$\|110001100\cdots\rangle$
×	×	$\|11101110\cdots\rangle$

The first two situations represent that particles can only hop between odd or even bonds, with evolution governed by an isolated part (e.g., The Hilbert space containing the example state $|01100110\cdots\rangle$ only permits transitions between odd bonds). Type three is for those particles that are permitted to hop across both odd and even bonds, resulting in evolution jointly driven by both parts of the Hamiltonian. The last one cannot evolve due to the absence of allowed hopping channels. Below we discuss the difference between long-lived revivals under isolated parts and double parts.

3. Single Scar under Resonant Regime. The restricted Hilbert space graph has been used to analyze the dynamic structure.[53] Because the evolution of system depends on four adjacency sites, we take four adjacency sites as a cell. Each cell can take the values $|+\rangle = |1100\rangle$ and $|-\rangle = |1010\rangle$. We focus on the largest connected component (the maximal disconnected subsector $\mathcal{K}$, where the number of quantum states is maximized with a given system size), which is the one containing the $|\mathbb{Z}_2\rangle$ state (the periodically arranged state $|101010\cdots\rangle$). In Fig. 1(c), we plot the restricted Hilbert space (the largest $\mathcal{K}$) of the effective model for $L = 12$. Each vertex stands for a basis state. Two vertices are connected by the nonzero matrix element between the two corresponding basis states. Basis states hopping inside cells constitute a form of a tower, which are labeled in red. On the other hand, basis states hopping between cells are outside the tower, and are labeled in blue. Taking into consideration the intercommunity of the odd part and the even part, in what follows we calculate the dynamic properties and eigenstates of only isolated even part of Hamiltonian to further investigate the system with exact diagonalization[55] (the results of the odd part and the even part are high consistent).

The Hamiltonian possesses a symmetry F related to spatial inversion and particle-hole exchange, having eigenvalues ±1 (see SM). It can be expressed by $F = \Pi_{j=1}^{L/2} F_j$, here

$$F_j = n_j(1-n_{L+1-j}) + (1-n_j)n_{L+1-j} + c_j^\dagger X_{j,L-j} c_{L+1-j}^\dagger + c_{L+1-j} X_{j,L-j} c_j \tag{3}$$

with $X_{j,L-j} = (2n_j - 1)(2n_{j+1} - 1)\cdots(2n_{L-j} - 1)$. Furthermore, the model has another symmetry $M = e^{i\pi \sum_j n_{2j+1}}$ anticommutes with the Hamiltonian, and therefore each eigenstate $|\psi\rangle$ with energy $E \neq 0$ has a partner $M|\psi\rangle$ with energy $-E$. Here we calculate the average ratio of consecutive level spacing and corresponding level spacing distribution in Fig. 2(a).

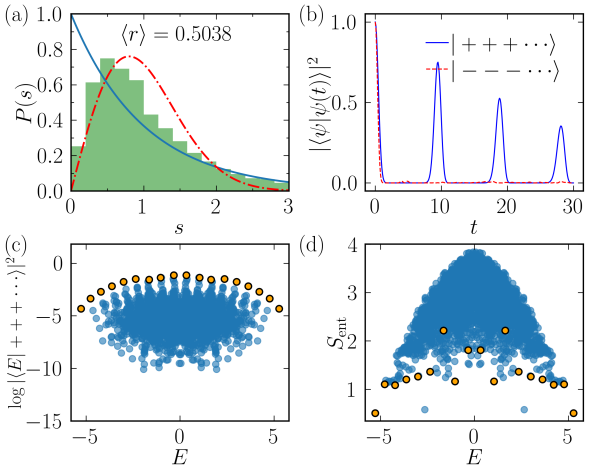

Fig. 2. (a) The level spacing distribution with $L = 44$. The blue solid (red dash-dot) curve denotes Poisson distributions (Wigner–Dyson distributions). The $\langle r\rangle$ value of the distribution given in the figure is close to the Wigner–Dyson result, $\langle r\rangle \approx 0.5038$. (b) Fidelity dynamics with $L = 36$ for $|+++\cdots\rangle$ and $|----\cdots\rangle$ states. (c) Overlap between eigenstates and $|+++\cdots\rangle$ state as a function of corresponding energy E. (d) Entanglement entropy $S_{\rm ent}$. The orange dots indicate the eigenstates sitting at the top of each tower of states. System size is $L = 36$ and the hopping strength is $J_{\rm e} = J_{\rm o} = 1$.

We find the level spacing distribution $P(s)$ follows the Wigner–Dyson distribution, while $\langle r\rangle = 0.5038$ is consistent with the Gaussian orthogonal ensemble.[56–60] Taken together, these facts suggest that the even part of Hamiltonian Eq. (2) is ergodic.

The practical determination of QMBS is that some special initial states manifest initial memory with the development of time, while the majority of initial states thermalize and do not keep initial memory.[53] Fidelity dynamics $|\langle\psi|\psi(t)\rangle|^2$ is a proper quantity to detect QMBS in Fig. 2(b) for the even part of Hamiltonian. Damped periodic revivals are clearly visible in the $|+++\cdots\rangle$ state with the period $T \approx 10$. On the contrary, the $|----\cdots\rangle$ state does not revive and the initial information is lost. Apart from the fidelity calculation, we can also verify QMBS by means of mapping to the PXP model (see SM for details).

To provide further insights into the structure of special eigenstates, we study the entire many-body spectrum according to the overlap with special eigenstates.[47] Figure 2(c) illustrates the scatter plot of the overlap $|\langle E|+++\cdots\rangle|^2$ between the initial state $|+++\cdots\rangle$ and eigenstates $|E\rangle$ on a log scale versus the eigenenergy. The majority of eigenstates huddle together, while some special states are distinguished by atypically high overlaps with the $|+++\cdots\rangle$ state. The energy separation between the special states stays approximately constant near zero energy and is given by 0.66; thus the revival period is $T = 9.52$, which is consistent with the estimated period above.

It is well known that for highly excited ETH eigenstates, the entanglement entropy obeys the volume law, scaling proportionally to the volume.[47,61] As we will see, entanglement properties of QMBS special eigenstates are

dramatically different. Figure 2(d) shows the entanglement entropy of the entire eigenstates. The majority of eigenstates are consistent with the thermalization assumption. However, those special states labelled by the red dots which have high overlaps with the initial state, exhibit apparently low entanglement entropy, causing an ETH violation.

4. Nested Scar under Resonant Regime. In contrast to the investigations on QMBS under the isolated part of the Hamiltonian, those under the double parts of the Hamiltonian need to consider Hilbert space fragmentation in two independent subspaces. In this case, initial states play an important role in the evolution and ergodicity. Specifically speaking, evolutions only take place in the odd (even) part of Hilbert spaces if some parts of the initial states can match those acting under the odd (even) part of the Hamiltonian. Based on this understanding, the initial state $|\psi_{\text{dimer}}\rangle$ is set as the combination of odd and even parts: $|\psi_{\text{dimer}}\rangle = |11001100\cdots\rangle \otimes |0\rangle \otimes |11001100\cdots\rangle$ $(|+\cdots++0++\cdots+\rangle)$. Interestingly, the initial state with a middle additional site of empty occupancy, which introduces the combination of double parts, will exhibit unique revival behaviours.

For simplicity, without loss of generality, we set the hopping of the even part $J_{\text{e}} = 1.0$ as the energy unit and change the hopping of the odd part J_{o} for different results. Figures 3(a) and 3(b) show the fidelity dynamics for combined initial state $|\psi_{\text{dimer}}\rangle$. As we can see, fidelity keeps revivals in both $J_{\text{o}} = 2.0$ and $J_{\text{o}} = 0.1$, which indicates that the dimerized Hamiltonian is nonergodic. Since the combined initial state hosts long-lived revival under either isolated odd or even part Hamiltonian, the total evolution still shows nonergodic behavior. For $J_{\text{o}} = 2.0$ in Fig. 3(a), the dynamics of fidelity shows clear revivals with a period of $T_{\text{dimer}} \approx 10$, similar to the properties typically exhibited by quantum scar states.[25,47,49,53] However, for $J_{\text{o}} = 0.1$ in Fig. 3(b), the revival period increases approximately ten times. To more intuitively illustrate the different revival periods, we plot in the insets the Fourier transforms (from the time domain to the frequency domain f) of the fidelity dynamics under different parameters. The discrete Fourier transform of a time-domain signal is periodic, with the first half of its spectrum representing positive frequencies and the second half corresponding to negative frequencies. To more clearly identify frequency peaks, we computed the single-sided spectrum $|P(f)|$. The inset in Fig. 3(a) shows the maximal spectrum $|P(f)|$ at frequency $f = 0.1$, indicating that the system has a period of $T = 10$. Similarly, for $J_{\text{o}} = 0.1$, the frequency corresponding to the maximal amplitude is $f = 0.01$, so the period is ten times that of the previous case for $J_{\text{o}} = 2.0$. This can be interpreted by the commutation of the two dimerized Hamiltonian parts, i.e., $[H_{\text{odd}}$ and $H_{\text{even}}] = 0$, which ensures that the evolution of the isolated part of Hamiltonian is independent of the other one, giving rise to period-renormalized revivals and the nested pattern. In other words, the total period of fidelity dynamics in the dimerized Hamiltonian is the lowest common multiple of the period of fidelity dynamics in the isolated part of the Hamiltonian. For example, $J_{\text{o}} = 2.0$ with a half period makes no difference to the total period compared with Fig. 2(b), while $J_{\text{o}} = 0.1$ renormalizes the total period to ten times. Moreover, the amplitudes of revivals under the double parts of the Hamiltonian are obviously less than those under the isolated part of the Hamiltonian because the total amplitudes of revivals come from the production of two isolated parts.

The fidelity computed earlier represents a global observable. To better characterize the Hamiltonian dimerization and align with experimental feasibility, figures 3(c) and 3(d) present the time evolution of local observables n_2 (local occupation of lattice site 2) and n_{23} (local occupation of lattice site 23) at $J_{\text{e}} = 1$ and $J_{\text{o}} = 0.1$ for the combined initial state $|\psi_{\text{dimer}}\rangle$. Both time evolutions of local occupation numbers n_2 and n_{23} exhibit periodic revivals, demonstrating nearly identical revival patterns. The sole distinction lies in their periods: one with $T \approx 10$ and the other with $T \approx 100$. The distinct evolution periods of different occupation sites along the same chain can be explained by Hamiltonian dimerization. Due to the independent evolution of the even and odd parts

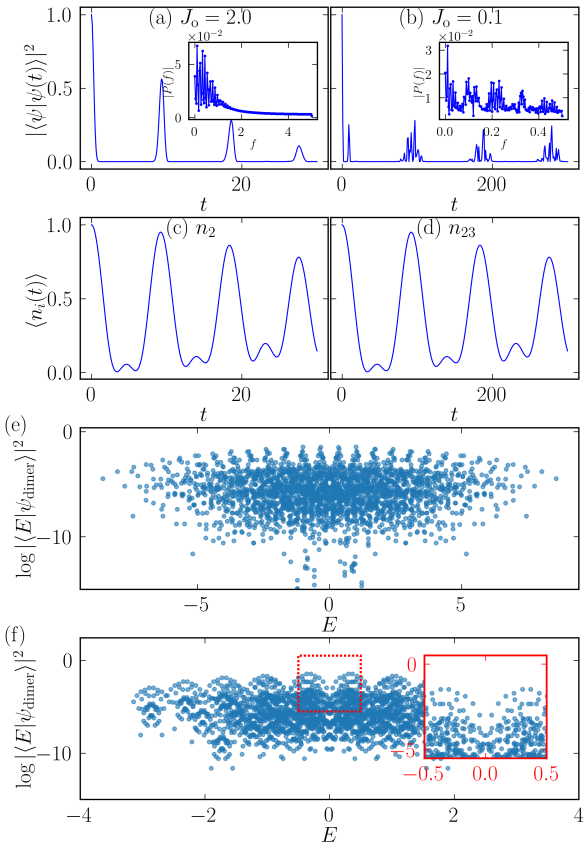

Fig. 3. Fidelity dynamics with $L = 41$ for $|\psi_{\text{dimer}}\rangle$ defined in the text and $J_{\text{e}} = 1$ at odd sites hopping (a) $J_{\text{o}} = 2.0$ and (b) $J_{\text{o}} = 0.1$. The insets respectively show the Fourier transforms from the time domain to the frequency domain for $J_{\text{o}} = 2.0$ and $J_{\text{o}} = 0.1$. The time evolution of local occupation numbers (c) n_2 and (d) n_{23} corresponds to the parameters in (b). The overlap with $J_{\text{e}} = 1.0$, (e) $J_{\text{o}} = 2.0$ and (f) $J_{\text{o}} = 0.1$ between eigenstates and combined initial state $|\psi_{\text{dimer}}\rangle$ as a function of corresponding energy E. The inset shows energies around zero at $J_{\text{e}} = 1$ and $J_{\text{o}} = 0.1$. The system size is $L = 41$.

of the Hamiltonian, the dynamics of n_2 depends solely on the even part of Hamiltonian, while n_{23} evolves according to the odd part of the Hamiltonian alone. Consequently, their respective revival periods are determined by the corresponding hopping parameters $J_e = 1.0$ and $J_o = 0.1$.

As shown in Fig. 3(b), there are additional revivals consistent with the original period in every revival. It can be explained by the overlap between eigenstates and special initial state. In Fig. 3(e), the large overlap states also form a band on top of all states, and $J_o = 2.0$ makes no change to the energy separation; thus, the total period remains consistent with that in the former text. However, for $J_o = 0.1$ in Fig. 3(f), the large overlap states form a set of towers on top of all states, and every tower consists of several points with equal energy spacing. This differs from the properties manifested in the overlap of typical quantum scar states.[49] After comparing the energy separation in detail, we find that the energy separation of each tower is 0.66, which is consistent with the uniform regime, and the inner energy spacing is around 0.06, contributing to the large-period revivals. In brief, the nested QMBS band in the two-fold PXP model is tunable in a relative regime due to the commutation of two dimerized parts, and it can provide a better understanding of Hamiltonian dimerization.

5. Discussion. From an experimental point of view, we note that all major ingredients of the proposed scheme can be readily realized using the existing techniques of ultracold atoms. We consider a concrete example, e.g., a single-component ultracold Fermi gas of ^{40}K atoms; here we choose the hyperfine state $|F, m_F\rangle = |9/2, -7/2\rangle$ due to its p-wave interaction, which has been well implemented in previous experiments.[62–64] We load the atoms into a 1D optical lattice with the wavelength $\lambda_L = 826\,\text{nm}$ and trap depth $V_0 = 9E_R$. The recoil energy of such an optical lattice is $E_R = h^2/(2m\lambda_L^2) \approx 7.26\,\text{kHz}$. Using the technique of p-wave Feshbach resonance, we can get a bare p-wave interaction strength $g_p = 550E_R$. After the above setups, the system parameters used in the main text can be determined as hopping amplitudes $J_o = J_e \approx 0.0192E_R$ and nearest-neighbor interaction strength $U \approx 0.2265E_R \gg J_o, J_e$. For different hopping amplitudes, we can synthesize the staggered hopping by applying a double-well structure to the optical lattice potential or using optical fields, which have also been widely applied in ultracold atoms.[65–68] The recent emulation of the Hubbard model with tilted magnetic fields Δ using ultracold atoms trapped in optical lattices[52,69] allows us to predict that our physics investigations can be experimentally verified with quantum simulators. In particular, similar many-body scarring in a Bose–Hubbard model with unit filling and a linear tilted potential was also recently observed.[70]

For the convenience of experimental implementation, we calculate the occupancy imbalance $\mathcal{I} = N_o - N_e/N_o + N_e$, which corresponds to staggered magnetization in this system.[71] Here, N_o (N_e) is the total number of fermions on the odd (even) sites. The density imbalance is one of the feasible quantities that can be experimentally measured with current techniques. For the isolated part of the Hamiltonian in Fig. 4(a), most of the initial states reach a fixed value rapidly, consistent with the thermalization of the system. The fixed value of thermalization ≈ 0.47, which is not zero. By contrast, QMBS remains persistent oscillations of the occupancy imbalance, whose oscillation period matches half the wave function revival period. For the double part of the Hamiltonian in Fig. 4(b), the occupancy imbalance of the thermalization state is fixed at zero, and QMBS also shows robust oscillations in this regime.

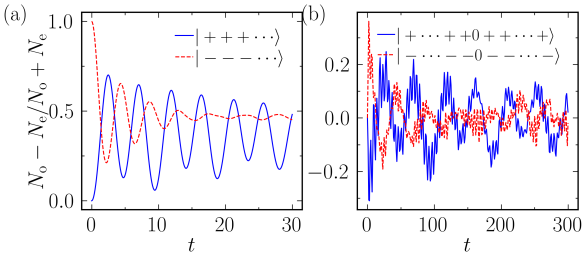

Fig. 4. (a) The time evolution of the occupancy imbalance with initial state $|+++\cdots\rangle$ and $|---\cdots\rangle$. The system size is $L = 36$, $J_e = J_o = 1.0$. (b) The time evolution of the occupancy imbalance with initial state $|+\cdots++0++\cdots+\rangle$ and $|-\cdots--0--\cdots-\rangle$. The sysytem size is $L = 41$, $J_e = 1.0$, and $J_o = 0.1$.

In summary, we have investigated the Hamiltonian dimerization and induced QMBS in the spinless Fermi–Hubbard model with a strong-tilted field. The properties of QMBS in one-dimensional quantum systems with a tilted field remain under active investigation. On the one hand, reference [53] used a spinful Fermi–Hubbard model to argue that the scars originate from a subgraph, representing a free spin-1 paramagnet. The same system has been realized in Ref. [52]. On the other hand, reference [70] realizes QMBS in a tilted Bose–Hubbard optical lattice and develops a quantum-interference protocol for measuring the entanglement entropy. In contrast to the previous studies, our system consists of spinless fermions with a unique four-site-dependent hopping structure, which gives rise to the distinctive Hamiltonian dimerization in our work. In comparison with conventional QMBS, the nested scar states we investigate exhibit two distinctive features: the period of quantum revivals exhibiting a nested revival pattern and the overlap presenting a nested energy spectrum structure. Furthermore, we investigated the off-resonance regime where quantum scar states in the system progressively vanish as the detuning strength increases.

In future work, it would be intriguing to explore other systems exhibiting intrinsic Hamiltonian dimerization and extend this framework to 2D geometries and non-Hermitian scenarios. Notably, non-Hermitian many-body scarring has been proposed in the PXP model by introducing an imaginary magnetic field.[72]

Acknowledgements. We are particularly grateful to Professor Zlakto Papić for the fruitful comment. This work was supported by the National Key R&D Program of China (Grant No. 2023YFA1406002) and the Innovation Program for Quantum Science and Technology (Grant No. 2021ZD0301200).

References

[1] Kinoshita T, Wenger T, and Weiss D S 2006 *Nature* **440** 900

[2] Schreiber M, Hodgman S S, Bordia P, Lüschen H P, Fischer M H, Vosk R, Altman E, Schneider U, and Bloch I 2015 *Science* **349** 842

[3] Kaufman A M, Tai M E, Lukin A, Rispoli M, Schittko R, Preiss P M, and Greiner M 2016 *Science* **353** 794

[4] Choi J Y, Hild S, Zeiher J, Schauß P, Abadal A R, Yefsah T, Khemani V, Huse D A, Bloch I, and Gross C 2016 *Science* **352** 1547

[5] Smith J, Lee A, Richerme P, Neyenhuis B, Hess P W, Hauke P, Heyl M, Huse D A, and Monroe C 2016 *Nature* **12** 907

[6] Kaplan H B, Guo L, Tan W L, De A, Marquardt F, Pagano G, and Monroe C 2020 *Phys. Rev. Lett.* **125** 120605

[7] Schindler P, Müller M, Nigg D, Barreiro J T, Martinez E A, Hennrich M, Monz T, Diehl S, Zoller P, and Blatt R 2013 *Nat. Phys.* **9** 361

[8] Chiaro B, Neill C, Bohrdt A, Filippone M, Arute F, Arya K, Babbush R, Bacon D, and Bardin J 2022 *Phys. Rev. Res* **4** 013148

[9] Fitzpatrick M, Sundaresan N M, Li A C Y, Koch J, and Houck A A 2017 *Phys. Rev. X* **7** 011016

[10] Guo X Y, Yang C, Zeng Y, Peng Y, Li H K, H. Deng, Jin Y R, Chen S, Zheng D, and Fan H 2019 *Phys. Rev. Appl.* **11** 044080

[11] Ye Y, Ge Z Y, Wu Y, Wang S, Gong M, Zhang Y R, Zhu Q, Yang R, Li S, Liang F, Lin J, Xu Y, Guo C, Sun L, Cheng C, Ma N, Meng Z Y, Deng H, Rong H, Lu C Y, Peng C Z, Fan H, Zhu X, and Pan J W 2019 *Phys. Rev. Lett.* **123** 050502

[12] Deutsch J M 1991 *Phys. Rev. A* **43** 2046

[13] Srednicki M 1994 *Phys. Rev. E* **50** 888

[14] Srednicki M 1999 *J. Phys. A: Math. Gen.* **32** 1163

[15] Gornyi I V, Mirlin A D, and Polyakov D G 2005 *Phys. Rev. Lett* **95** 206603

[16] Basko D M, Aleiner I L, and Altshuler B L 2006 *Ann. Phys.* **321** 1126

[17] Nandkishore R and Huse D A 2015 *Annu. Rev. Condens. Matter Phys.* **6** 15

[18] Abanin D A and Papić Z 2017 *Ann. Phys.* **529** 1700169

[19] Alet F and Laflorencie N 2018 *C. R. Phys.* **19** 498

[20] Abanin D A, Altman E, Bloch I, and Serbyn M 2019 *Rev. Mod. Phys.* **91** 021001

[21] Serbyn M, Papić Z, and Abanin D A 2013 *Phys. Rev. Lett.* **111** 127201

[22] Ho W W, Choi S, Pichler H, and Lukin M D 2019 *Phys. Rev. Lett.* **122** 040603

[23] Turner C J, Desaules J Y, Bull K, and Papić Z 2021 *Phys. Rev. X* **11** 021021

[24] Bluvstein D, Omran A, Levine H, Keesling A, Semeghini G, Ebadi S, Wang T T, Michailidis A A, Maskara N, Ho W W, Choi S, Serbyn M, Greiner M, Vuletić V, and Lukin M D 2021 *Science* **371** 1355

[25] Turner C J, Michailidis A A, Abanin D A, Serbyn M, and Papić Z 2018 *Phys. Rev. B* **98** 155134

[26] Lin C J, Chandran A, and Motrunich O I 2020 *Phys. Rev. Res.* **2** 033044

[27] Mondragon-Shem I, Vavilov M G, and Martin I 2021 *PRX Quantum* **2** 030349

[28] Zhao H, Vovrosh J, Mintert F, and Knolle J 2020 *Phys. Rev. Lett.* **124** 160604

[29] Iadecola T, Schecter M, and Xu S 2019 *Phys. Rev. B* **100** 184312

[30] Chattopadhyay S, Pichler H, Lukin M D, and Ho W W 2020 *Phys. Rev. B* **101** 174308

[31] Mukherjee B, Nandy S, Sen A, Sen D, and Sengupta K 2020 *Phys. Rev. B* **101** 245107

[32] Bernien H, Schwartz S, Keesling A, Levine H, Omran A, Pichler H, Choi S, Zibrov A S, Endres M, Greiner M, Vuletić V, and Lukin M D 2017 *Nature* **551** 579

[33] Turner C J, Michailidis A A, Abanin D A, Serbyn M, and Papić Z 2018 *Nat. Phys.* **14** 745

[34] Choi S, Turner C J, Pichler H, Ho W W, Michailidis A A, Papić Z, Serbyn M, Lukin M D, and Abanin D A 2019 *Phys. Rev. Lett.* **122** 220603

[35] Khemani V, Laumann C R, and Chandran A 2019 *Phys. Rev. B* **99** 161101

[36] Michailidis A A, Turner C J, Papić Z, Abanin D A, and Serbyn M 2019 *Phys. Rev. Res.* **2** 022065

[37] Lin C J, Calvera V, and Hsieh T H 2020 *Phys. Rev. B* **101** 220304

[38] Bull K, Martin I, and Papić Z 2019 *Phys. Rev. Lett.* **123** 030601

[39] Kuno Y, Mizoguchi T, and Hatsugai Y 2020 *Phys. Rev. B* **102** 241115

[40] Serbyn M, Abanin D A, and Papić Z 2021 *Nat. Phys.* **17** 675

[41] Moudgalya S, O'Brien E, Bernevig B A, Fendley P, and Regnault N 2020 *Phys. Rev. B* **102** 085120

[42] Pakrouski K, Pallegar P N, Popov F K, and Klebanov I R 2020 *Phys. Rev. Lett.* **125** 230602

[43] O'Dea N, Burnell F, Chandran A, and Khemani V 2020 *Phys. Rev. Res.* **2** 043305

[44] Surace F M, Giudici G, and Dalmonte M 2020 *Quantum* **4** 339

[45] Moudgalya S, Regnault N, and Bernevig B A 2018 *Phys. Rev. B* **98** 235156

[46] Mark D K, Lin C J, and Motrunich O I 2020 *Phys. Rev. B* **101** 195131

[47] Schecter M and Iadecola T 2019 *Phys. Rev. Lett.* **123** 147201

[48] Sala P, Rakovszky T, Verresen R, Knap M, and Pollmann F 2020 *Phys. Rev. X* **10** 011047

[49] Moudgalya S, Bernevig B A, and Regnault N 2022 *Rep. Prog. Phys.* **85** 086501

[50] Khemani V, Hermele M, and Nandkishore R 2020 *Phys. Rev. B* **101** 174204

[51] Yang Z C, Liu F, Gorshkov A V, and Iadecola T 2020 *Phys. Rev. Lett.* **124** 207602

[52] Scherg S, Kohlert T, Sala P, Pollmann F, Hebbe Madhusudhana B, Bloch I, and Aidelsburger M 2021 *Nat. Commun.* **12** 4490

[53] Desaules J Y, Hudomal A, Turner C J, and Papić Z 2021 *Phys. Rev. Lett.* **126** 210601

[54] Kohlert T, Scherg S, Sala P, Pollmann F, Hebbe Madhusudhana B, Bloch I, and Aidelsburger M 2023 *Phys. Rev. Lett.* **130** 010201

[55] Sandvik A W 2010 *AIP Conf. Proc.* **1297** 135

[56] Buijsman W, Gritsev V, and Sprik R 2017 *Phys. Rev. Lett.* **118** 080601

[57] Bohigas O, Giannoni M J, and Schmit C 1984 *Phys. Rev. Lett.* **52** 1

[58] Robnik M 2016 *Eur. Phys. J. Spec. Top* **225** 959

[59] Victor B M and Tabor M 1977 *Proc. R. Soc. Lond. A.* **356** 375

[60] Atas Y Y, Bogomolny E, Giraud O, and Roux G 2013 *Phys. Rev. Lett.* **110** 084101

[61] Bianchi E, Hackl L, Kieburg M, Rigol M, and Vidmar L 2022 *PRX Quantum* **3** 030201

[62] Regal C A, Ticknor C, Bohn J L, and Jin D S 2003 *Phys. Rev. Lett.* **90** 053201

[63] Ticknor C, Regal C A, Jin D S, and Bohn J L 2004 *Phys. Rev. A* **69** 042712

[64] Günter K, Stöferle T, Moritz H, Köhl M, and Esslinger T 2005 *Phys. Rev. Lett.* **95** 230401
[65] Li X, Zhao E, and Vincent Liu W 2013 *Nat. Commun.* **4** 1523
[66] Greif D, Uehlinger T, Jotzu G, Tarruell L, and Esslinger T 2013 *Science* **340** 1307
[67] Atala M, Aidelsburger M, Lohse M, Barreiro J T, Paredes B, and Bloch I 2014 *Nat. Phys.* **10** 588
[68] Zhang S L and Zhou Q 2017 *Phys. Rev. A* **95** 061601
[69] Zhou Z Y, Su G X, Halimeh J C, Ott R, Sun H, Hauke P, Yang B, Yuan Z S, Berges J, and Pan J W 2022 *Science* **377** 311
[70] Su G X, Sun H, Hudomal A, Desaules J Y, Zhou Z Y, Yang B, Halimeh J C, Yuan Z S, Papić Z, and Pan J W 2023 *Phys. Rev. Res.* **5** 023010
[71] Chen Y and Cai Z 2020 *Phys. Rev. A* **101** 023611
[72] Chen Q, Chen S A, and Zhu Z 2023 *SciPost Phys.* **15** 052